Available online at www.sciencedirect.com
ScienceDirect
Journal of Catalysis 251 (2007) 281–294
JOURNAL OF CATALYSIS
www.elsevier.com/locate/jcat

Glycerol hydrogenolysis on carbon-supported PtRu and AuRu bimetallic catalysts

Erin P. Maris [a], William C. Ketchie [a], Mitsuhiro Murayama [b], Robert J. Davis [a,*]

[a] *Department of Chemical Engineering, University of Virginia, 102 Engineers Way, Charlottesville, VA 22904-4741, USA*
[b] *Department of Materials Science and Engineering, University of Virginia, 116 Engineers Way, Charlottesville, VA 22904-4745, USA*

Received 9 May 2007; revised 19 July 2007; accepted 11 August 2007

Abstract

Bimetallic PtRu and AuRu catalysts were prepared by a surface redox method in which Pt or Au was deposited onto the surface of carbon-supported Ru nanoparticles with an average diameter of 2–3 nm. Characterization by H_2 chemisorption, analytical TEM, and X-ray absorption spectroscopy at the Ru K-edge, Pt L_{III}-edge, and Au L_{III}-edge confirmed that Pt and Au were successfully deposited onto Ru without disrupting the Ru particles. Depression of the ethane hydrogenolysis rate over Ru after addition of Au provided further evidence of successful deposition. The bimetallic particles were subsequently evaluated in the aqueous-phase hydrogenolysis of glycerol at 473 K and 40 bar H_2 at neutral and elevated pH. Although monometallic Pt and Ru exhibited different activities and selectivities to products, the bimetallic PtRu catalyst functioned more like Ru. A similar result was obtained for the AuRu bimetallic catalyst. The PtRu catalyst appeared to be stable under the aqueous-phase reaction conditions, whereas the AuRu catalyst was altered by the harsh conditions. Gold appeared to migrate off the Ru and agglomerate on the carbon during the reaction in liquid water.

Keywords: Glycerol; Hydrogenolysis; Bimetallic catalysts; X-ray absorption spectroscopy; Transmission electron microscopy

1. Introduction

The primary feedstocks of renewable organic fuels, chemicals, and materials are and will be derived from biomass [1–4]. In particular, glycerol has been identified as a promising alternative to petroleum and natural gas for the production of commodity chemicals and materials [5]. Because glycerol is also the major byproduct of biodiesel production by transesterification of vegetable oil [6], using the growing supply of glycerol is a logical step in moving toward a more sustainable economy. One industrially relevant route for the conversion of glycerol to oxygenated chemicals involves hydrogenolysis to ethylene glycol, propylene glycol, and lactic acid, as shown in Scheme 1 [7,8].

Previous studies have demonstrated the effectiveness of heterogeneous catalysts in the hydrogenolysis of polyols to lower molecular weight glycols and acids [9–11]. Recent work in our laboratory has shown that Ru/C and Pt/C are catalysts for the hydrogenolysis of glycerol, where the selectivities to ethylene glycol and propylene glycol are a function of metal type and solution pH [12]. Other studies have shown that addition of a modifier, such as sulfur, can alter the activity and selectivity of glycerol hydrogenolysis catalysts [13,14]. Montassier et al. demonstrated that increasing coverage of sulfur on a Ru/C catalyst decreased the activity for glycerol hydrogenolysis under neutral pH but increased selectivity to propylene glycol [13]. These authors also observed a maximum in the ethylene glycol selectivity at a sulfur coverage of 25%. Lahr and Shanks [14] also investigated the effects of sulfur addition on glycerol hydrogenolysis over Ru/C at high pH, and found that higher sulfur loadings increased the selectivity to propylene glycol without altering the selectivity to ethylene glycol.

Hydrogenolysis reactions are well known to be structure sensitive; that is, the activity and selectivity depend on catalyst surface structure or particle size. However, it is not clear

* Corresponding author. Fax: +1 (434) 982 2658.
E-mail address: rjd4f@virginia.edu (R.J. Davis).

0021-9517/$ – see front matter
doi:10.1016/j.jcat.2007.08.007

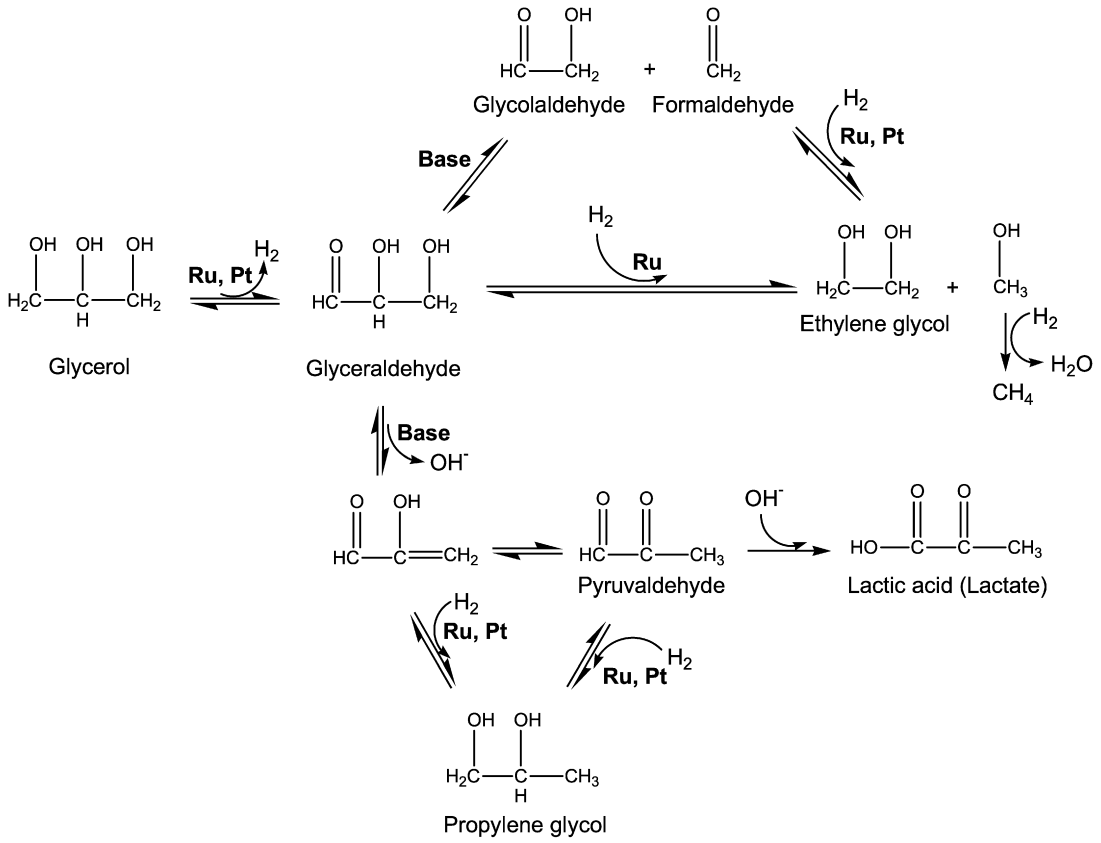

Scheme 1. Proposed mechanism of glycerol hydrogenolysis. Adapted from Ref. [12].

whether the role of sulfur in the study of glycerol hydrogenolysis is simple site-blockage of the Ru surface atoms that form an active ensemble or some other modification. Adsorbed sulfur has been suggested to electronically modify the Ru surface [13] and possibly inhibit a low-energy catalytic pathway to propylene glycol in favor of a higher energy pathway [14]; thus, the role of sulfur may involve both ensemble effects and electronic (or ligand) effects.

Bimetallic catalysts have been used to alter the activity and selectivity of various reactions, including hydrogenolysis reactions [15–19]. Moreover, Pt–Ru bimetallic catalysts are widely studied for potential use as anodes in fuel cell applications [19,20]. Although Ru and Pt are partially miscible in the bulk [21], they need not form an alloy to display synergistic catalytic activity [20]. As mentioned earlier, previous work in our lab has demonstrated clear differences between carbon-supported Ru and Pt catalysts for glycerol hydrogenolysis [12]. Because bimetallic catalysts can exhibit catalytic activities that surpass those of their monometallic analogues [18], we considered the evaluation of Pt–Ru bimetallic particles as a reasonable next step. Addition of Au has also been shown to alter the activity of Ru for ethane and propane hydrogenolysis [22]. Because Ru and Au are not miscible in the bulk [21], particular attention must be paid to catalyst synthesis and characterization of this bimetallic system. In previous studies of alkane hydrogenolysis on bimetallic Au–Ru catalysts, the depression of catalytic activity of Ru by addition of Au was considered primarily an ensemble effect instead of an electronic effect [22–24]; therefore, evaluation of Ru–Au bimetallic catalysts for glycerol hydrogenolysis is a logical test for ensemble effects.

In this work, we compare carbon-supported Pt–Ru and Au–Ru bimetallic catalysts to their monometallic analogues for the hydrogenolysis of glycerol under neutral conditions and at high pH. The catalysts were characterized by H_2 chemisorption, transmission electron microscopy, in situ X-ray absorption spectroscopy, and ethane hydrogenolysis so that catalyst structure could be related directly to activity and selectivity.

2. Experimental

2.1. Catalyst preparation

Activated carbon-supported Ru and Pt monometallic catalysts were obtained from Acros Organics and Sigma–Aldrich, respectively. The Ru/C (5 wt% Ru, 50% w/w water) catalyst was dried in air at 493 K overnight before use; Pt/C (3 wt% Pt) was used as received. Gold was supported on activated carbon by cation exchange. The activated carbon was first oxidized with aqueous sodium hypochlorite (NaClO) solution according to the method reported by Gallezot et al. [25]. The $[Au(en)_2]Cl_3$ (en = ethylenediamine) needed as a precursor for ion exchange was prepared according to the method of Block and Bailar [26]. To prepare the Au/C, 20 $cm^3\ g^{-1}$ of the oxidized carbon support was slurried with 1 M ammonium hydroxide (Alfa Aesar, 50% v/v), while bubbling N_2 through the mixture at ambient conditions. The appropriate amount of $[Au(en)_2]Cl_3$ was dissolved in

1 M ammonium hydroxide to form a 0.01 M solution and this solution was added dropwise to the carbon slurry. The resulting suspension was stirred at ambient conditions in the presence of bubbling N_2 for 24 h. The suspension was filtered and washed with distilled deionized water until no Cl^- could be detected with a 0.1 M $AgNO_3$ test. The catalyst was dried at ambient conditions overnight, followed by drying in air at 383 K for 2 h.

The Ru/C catalyst also was used as a precursor for the preparation of bimetallic Pt–Ru and Au–Ru catalysts by surface redox reactions [27–29]. For the preparation of the PtRu/C bimetallic catalyst, the parent Ru/C catalyst was slurried with 20 $cm^3\,g^{-1}$ 0.05 M HCl (Acros Organics) in a sealed glass reactor equipped with a magnetic stirrer. To remove air in the system, N_2 (GT&S, 99.998%) was bubbled through the slurry at room temperature for 1 h. To remove N_2 and reduce the Ru surface, H_2 (GT&S, 99.995%) was bubbled through the slurry for 2 h at 353 K. The appropriate amount of $H_2PtCl_6{\cdot}xH_2O$ (Acros Organics, 38.75 wt% Pt) was dissolved in 20 $cm^3\,g^{-1}$ of 0.05 M HCl and degassed by flowing N_2 through the solution for 1 h. The Pt precursor solution was added dropwise through a gas-tight syringe to the Ru/C slurry. Once the Pt precursor was added, the slurry was stirred for 1 h under bubbling H_2 at 353 K, then cooled to room temperature under H_2, after which the reactor was purged with N_2 before being exposed to air. The catalyst was filtered and washed with 6 L of distilled deionized water to remove residual Cl^-. The final filtrate tested negative for Cl^- using a 0.1 M $AgNO_3$ solution. The catalyst was allowed to dry in air at 393 K overnight. A bimetallic Au–Ru catalyst also was prepared in this manner, where $HAuCl_4$ (Aldrich) was used as the Au precursor. The catalysts are designated PtRu/C and AuRu/C in this work.

After preparation, the catalysts were heated at 2 K min^{-1} in H_2 (GT&S, 99.999%, purified using a Matheson 8371V palladium hydrogen purifier) flowing at 100 $cm^3\,min^{-1}$ to 523 K and held at that temperature for 4 h. The reduced catalysts were allowed to cool under H_2. Once room temperature was reached, a stream of He was passed over the catalyst bed, followed by slow exposure to air. The Ru, Au, and Pt weight loadings were determined by ICP analysis (Galbraith Laboratories, Knoxville, TN).

2.2. H_2 chemisorption

The metal dispersion and particle size of the Ru/C and Pt/C catalysts were evaluated by H_2 chemisorption performed on a Micromeritics ASAP 2020 chemisorption analyzer at 308 K in the pressure range of 10–450 Torr. Before chemisorption, the catalysts were heated from ambient conditions to 523 K at 4 K min^{-1} in flowing H_2 (GT&S 99.999%). The catalysts were reduced in H_2 at 523 K for 90 min, followed by evacuation at 523 K for 4 h. After cooling to 308 K, the catalysts were evacuated again for 2 h followed by analysis at 308 K. Surface Ru and Pt were evaluated by the total amount of H_2 adsorbed at 303 K extrapolated to zero pressure, assuming a stoichiometry (H/M_{surf}, M = Ru, Pt) equal to unity. Dihydrogen adsorption also was performed on the bimetallic PtRu/C and AuRu/C catalysts to compare the amount of hydrogen adsorbed per gram of catalyst with that on the parent Ru/C catalyst.

2.3. Transmission electron microscopy

The catalyst particle size and morphology were examined by bright-field and dark-field transmission electron microscopy (TEM) using a JEOL 2010F transmission electron microscope operating at 200 kV and equipped with a Gatan imaging filter (GIF). Samples were prepared by suspending the catalyst in ethanol and agitating in an ultrasonic bath for 2 h. The suspension was allowed to sit overnight so that larger particles could settle out. Two drops of the suspended catalyst were applied to a copper mesh grid with lacy carbon film, with the ethanol evaporating in between drops. Images were recorded on film and on a slow-scan CCD camera that permitted analysis with the Gatan Digital Micrograph software package. Energy dispersive X-ray spectroscopy (EDS) was carried out using an Oxford Instruments model 6498 detector and the NIST Desktop Spectrum Analyzer software [30]. For analysis of individual particles, the electron beam was focused to a diameter that was slightly less than the diameter of the particle being investigated. Metal particle size distributions were determined using ImageJ software [31].

2.4. X-ray absorption spectroscopy

The X-ray absorption spectroscopy (XAS) was performed at the National Synchrotron Light Source, Brookhaven National Laboratory. The storage ring operated at 2.8 GeV with a ring current of 150–300 mA. Data were collected on beamline X-18B operating in transmission mode at the Ru K-edge (22.118 keV) with a beam spot size of 0.5 mm × 10 mm, the Pt L_{III}-edge (11.564 keV), and the Au L_{III}-edge (11.919 keV) with a spot size of 1 mm × 10 mm.

Samples were initially pressed into a copper holder and analyzed in a sample cell that allowed for heating to 473 K at 4 K min^{-1} under flowing H_2 (g). After 2 h at 473 K, the samples were cooled to 298 K under H_2 (g) flow. For each sample, a minimum of 3 scans was collected at 298 K over the appropriate energy range. A second in situ sample cell with its attached flow system (described in Ref. [32]) was used to analyze various catalysts during aqueous treatment. The samples were placed into a 1.5 mm × 20 mm × 6 (or 3) mm (X-ray path length) sample holder that was then sealed with poly-ether-ether-ketone disk windows on both sides to allow for the transmission of photons. The cell enabled data collection while an aqueous solution saturated with 40 bar H_2 was pumped through a packed catalyst bed heated to 473 K. The flow system comprised a vessel filled with 60 cm^3 of 0.4 M NaOH aqueous solution that was first purged by N_2, then pressurized with 40 bar H_2. The H_2-saturated solution (40 bar) was then pumped through the packed bed of catalyst at a rate of 1.0 $cm^3\,min^{-1}$ while being heated to 473 K. The X-ray scans were collected while the solution flowed through the sample at 473 K.

The extended X-ray absorption fine structure (EXAFS) findings were analyzed using the WinXAS software package [33].

Between 3 and 6 scans were energy-referenced to a Ru powder, a Pt foil, or an Au foil placed between the transmission and reference ion chambers, then averaged before analysis. The first-shell Ru–Ru amplitude function and phase shift were extracted from a Ru/Al_2O_3 (17.6 wt% Ru) sample. The Ru reference was assumed to have the bulk crystallographic values of the Ru hcp structure with a first-shell coordination number (CN) of 12 and nearest-neighbor distance of 2.68 Å. For analysis of the EXAFS above the Pt L_{III}-edge, the energy reference and the first-shell Pt–Pt amplitude function and phase shift were extracted from a 4-μm Pt foil (Goodfellow, 99.95%) that was assumed to have the bulk crystallographic values of the Pt fcc structure with a first-shell CN of 12 and nearest-neighbor distance of 2.78 Å. For analysis of the EXAFS above the Au L_{III}-edge, the energy reference and the first-shell Au–Au amplitude function and phase shift were extracted from a 5-μm Au foil (Goodfellow, 99.9%). The foil was assumed to have the bulk crystallographic values of the Au fcc structure with a first-shell CN of 12 and nearest-neighbor distance of 2.88 Å. The experimental data were used to calibrate the theoretical photoelectron scattering amplitude and phase-shift functions for Ru, Pt, and Au calculated using FEFF8.2 [34]. The amplitude and phase-shift functions for the heterogeneous absorber-scatterer pairs (Ru–Pt and Ru–Au) also were generated using FEFF8.2. For samples evaluated at 298 K, data in the k-range of 3–15 $Å^{-1}$ were used for analysis, whereas for the samples examined under aqueous conditions at 473 K, data in the k-range of 3–14 $Å^{-1}$ were used. Curve fitting was performed in both R-space and k-space with k^1 and k^3 weighting, and the average of these four values is reported herein. The fitting procedure results in an estimated accuracy of ±10% for the first-shell CN, ±0.01 Å for interatomic distances, and ±10% for the Debye–Waller factor [35]. The physical constraints necessary for bimetallic fitting set forth by Via et al. [36] were maintained during the fitting process.

2.5. Ethane hydrogenolysis

The hydrogenolysis of ethane was conducted using a fixed-bed quartz tubular reactor flow system operating at 473 K and atmospheric pressure. All data were collected at a total flow rate of approximately 45 $cm^3\,min^{-1}$, where the catalyst amounts were adjusted to maintain ethane conversions <20%. Gas flow rates were maintained using mass flow controllers (Brooks Instruments, series 5850E) to deliver a stream containing 10 mol% ethane (GT&S, >99.95%), 33 mol% H_2 (GT&S, 99.999%), and He (GT&S, 99.9995%) as balance. The reactor effluent was analyzed by gas chromatography (GC) using an HP 5890 gas chromatograph equipped with an Alltech CTR1 column and a thermal conductivity detector (TCD). Before collection of kinetic data, the catalysts were reduced in situ by flowing 15 $cm^3\,min^{-1}$ H_2 at 473 K for 1 h.

2.6. Glycerol hydrogenolysis

Glycerol hydrogenolysis reactions were conducted semi-batchwise in a 300-ml stainless steel reactor (Parr Instruments) equipped with an electronic temperature controller, a mechanical stirrer, a catalyst addition device, and a dip tube for periodic sampling of the liquid phase. In a typical reaction, glycerol (Acros Organics, 99%) was diluted with distilled deionized water to form a 1 wt% solution. Then 150 ml of this solution was loaded into the reactor along with the appropriate amount of NaOH (Mallinckrodt) when necessary. When the monometallic catalysts were used, the appropriate amount of either Ru/C or Pt/C was loaded into the catalyst addition device to maintain a substrate/surface metal (S/M_{surf}) ratio of approximately 700. In studies of the bimetallic catalysts, the same mass of either PtRu/C or AuRu/C was used relative to the monometallic Ru/C case, to maintain comparable Ru loadings. Glycerol hydrogenolysis also was investigated with physical mixtures of the monometallic catalysts. In the case of Ru/C and Pt/C, the same mass of Ru/C was used as in the monometallic case; however, the appropriate amount of Pt/C was added to equal the amount of Pt present in the PtRu/C on a surface Pt atom basis. The number of surface Pt atoms present in the Pt/C catalyst was determined by H_2 chemisorption and it was assumed that all Pt atoms in the bimetallic catalyst were on the surface. In the case of Ru/C mixed with Au/C, the same mass of Ru/C was used as in the monometallic case, and sufficient Au/C was used to maintain a total Au loading equivalent to that in the AuRu/C catalyst.

After the catalysts were loaded into the catalyst addition device, the reactor was sealed and flushed with flowing N_2 (GT&S, 99.998%) at 1 bar for 10 min to remove air in the headspace. To remove the N_2, the reactor was subsequently flushed with flowing H_2 (GT&S, 99.995%) at 2 bar for 20 min. The reactor was then pressurized to 5 bar with H_2 and heated under moderate agitation (100 rpm) to a final reaction temperature of 473 K. Once this temperature was reached, an initial liquid sample was removed to mark the start of the reaction. Catalyst was subsequently introduced into the reaction medium through the catalyst addition device, the pressure was increased to 40 bar with H_2, and the rate of agitation was increased to 475 rpm. The reaction was allowed to proceed under these conditions for 5 h while liquid samples were periodically removed. The reactor was back-filled with H_2 after each sample to maintain constant pressure. Liquid samples were analyzed by high performance liquid chromatography (HPLC) using a ThermoSeparations Products (TSP) AS1000 autosampler equipped with a TSP P2000 pump, an Aminex HPX-87H (Bio Rad) column, a Waters R-401 refractive index detector, and Millennium data acquisition software. The HPLC column was maintained at 333 K, with a mobile phase of 5 mM H_2SO_4 flowing at 0.7 $ml\,min^{-1}$. The major liquid-phase products observed were ethylene glycol, propylene glycol, lactate, and formate; other byproducts detected in trace amounts by HPLC included glyceraldehyde, methanol, and ethanol.

At the conclusion of the 5 h reaction, the reactor was allowed to cool to room temperature. Gas samples in the headspace were removed by a gas-tight syringe and analyzed for CO_2 and CH_4 by GC, using an HP 5890 gas chromatograph equipped with an Alltech CTR1 column and TCD.

Table 1
Results from elemental analysis, H_2 chemisorption, and electron microscopy

Catalyst	Metal loading (wt%)	Atomic ratio (M/Ru)[a]	H_{ads}/g_{cat}	H/M[b]	H_2 chem. particle diameter (nm)[c]	TEM particle diameter (nm)	Surface averaged diameter (nm)[d]
Ru/C	5.0[e]	–	21 ± 0.78	0.43	2.3	2.6	3.1
Pt/C	3.0[e]	–	6.6 ± 1.1	0.43	2.3	2.5	2.8
Au/C	5.3	–	–	–	–	–	–
PtRu/C	1.9 (Pt), 4.7 (Ru)	0.21	14 ± 0.86	0.30	3.3	3.3	3.6
AuRu/C	0.85 (Au), 5.0 (Ru)	0.087	8.2 ± 0.62	0.17	–	2.9	5.8

[a] M denotes either Pt or Au.
[b] M denotes either Ru or Pt.
[c] Calculated as the inverse of the metal dispersion as determined by H_2 chemisorption.
[d] Determined by TEM as $(\sum d^3)/(\sum d^2)$.
[e] Metal loading provided by manufacturer.

3. Results and discussion

Table 1 summarizes the elemental composition and hydrogen adsorption capacity of the various samples. The hydrogen adsorption capacity per gram of catalyst (H_{ads}/g_{cat}) for each sample was determined by extrapolation of the linear portion of the isotherm to zero pressure. The monometallic Ru/C sample exhibited the highest hydrogen capacity, followed, in order, by PtRu/C, AuRu/C, and Pt/C. Note that Pt/C had a lower capacity than Ru/C because of its lower metal loading; on a per metal atom basis, the two samples had comparable hydrogen uptakes. The similar dispersion of the monometallic Ru/C and Pt/C samples (43%) corresponds to an average metal particle diameter of about 2.3 nm. Dihydrogen chemisorption was not attempted on the monometallic Au/C, because it is well known that Au does not dissociatively adsorb H_2 [37]. It is interesting that the PtRu/C sample had a lower uptake than the monometallic Ru/C sample. Moreover, the addition of Au to Ru/C resulted in a 2.5-fold decrease in hydrogen uptake. If every Au atom were deposited on the Ru surface, then the ratio of surface Au to surface Ru would be 0.20. The decrease in hydrogen capacity on the AuRu/C sample should be at most only 20%, yet we observed a more substantial suppression of adsorption. Consequently, we evaluated the particle sizes for the bimetallic samples by TEM.

Table 1 reports the mean particle diameter and surface average diameter for several of the samples as determined by electron microscopy. Particle size distributions (PSDs) were obtained by measuring at least 200 particles over multiple areas for each sample. Examination of Table 1 shows good agreement between the particle sizes for the monometallic samples determined by H_2 chemisorption and TEM. Representative micrographs are given for the PtRu/C and AuRu/C bimetallic samples, along with their corresponding EDS spectra and PSDs in Figs. 1 and 2. For the PtRu/C bimetallic sample, the particle size distribution was fairly narrow, in good agreement with the mean particle diameter and surface-averaged particle diameter data reported in Table 1. The addition of Pt to Ru/C resulted in a slight increase in the mean particle diameter, likely due to the deposition of Pt onto the Ru surface. The EDS of more than 10 individual particles revealed the presence of both Ru and Pt in each case; a representative EDS spectrum obtained from an individual particle is provided in Fig. 1a. The AuRu/C sample had a broader PSD, as shown in Fig. 2, resulting in a larger difference between the mean and the surface-averaged particle diameter than that reported in Table 1. The particle density was highest in the 1.5–3.0 nm particles; EDS over an average area of these small particles revealed primarily Ru, as shown in Fig. 2a. As shown in Fig. 2b, mid-range particles (5–10 nm) contained both Au and Ru, and larger particles (>10 nm) contained primarily Au.

These results indicate that although some Au was deposited onto the Ru particles, significant deposition and growth of Au monometallic particles occurred on the carbon support. In summary, electron microscopy of the bimetallic catalysts confirmed that Pt and Au were successfully deposited onto Ru, with a greater degree of interaction for Pt.

X-ray absorption spectroscopy also was used to characterize the catalyst samples. Inspection of the X-ray absorption near-edge spectra at the Ru K-edge, Pt L_{III}-edge, and Au L_{III}-edge revealed that after sample preparation, Au remained in a reduced metallic state, whereas Ru and Pt both were in an oxidized state. However, treatments under both H_2 (g) and H_2-saturated aqueous solutions at 473 K were able to reduce the Ru and Pt to a metallic state.

Representative χ data with k^3 weighting are presented in Fig. 3 for the PtRu/C sample. The Fourier-transformed k^3-weighted χ functions for the PtRu/C sample are also presented in Fig. 4. The EXAFS fitting results for all of the samples are summarized in Table 2. Treatment of the monometallic samples in H_2 (g) resulted in first-shell Ru–Ru and Pt–Pt CNs of 8.8 and 8.6, respectively, corresponding to a particle size of approximately 2 nm [38]. This is in good agreement with the particle sizes determined by H_2 chemisorption and TEM. The Ru–Ru first-shell CN remained essentially constant (8.8 ± 0.4) for all of the bimetallic samples, regardless of pretreatment. We previously reported that Ru particles are stable on an activated carbon support under aqueous-phase conditions [32,39]. Analysis of the EXAFS for the Pt/C sample revealed that treatment under aqueous-phase conditions increased the Pt–Pt first-shell CN from 8.6 to 10.4, which is consistent with growth of the Pt particles. Microscopy of Pt/C recovered after use in the hydrogenolysis of glycerol in the presence of 0.8 M NaOH at 473 K and 40 bar H_2 confirmed an increase in the average particle diameter from 2.5 to 3.9 nm and an increase in the

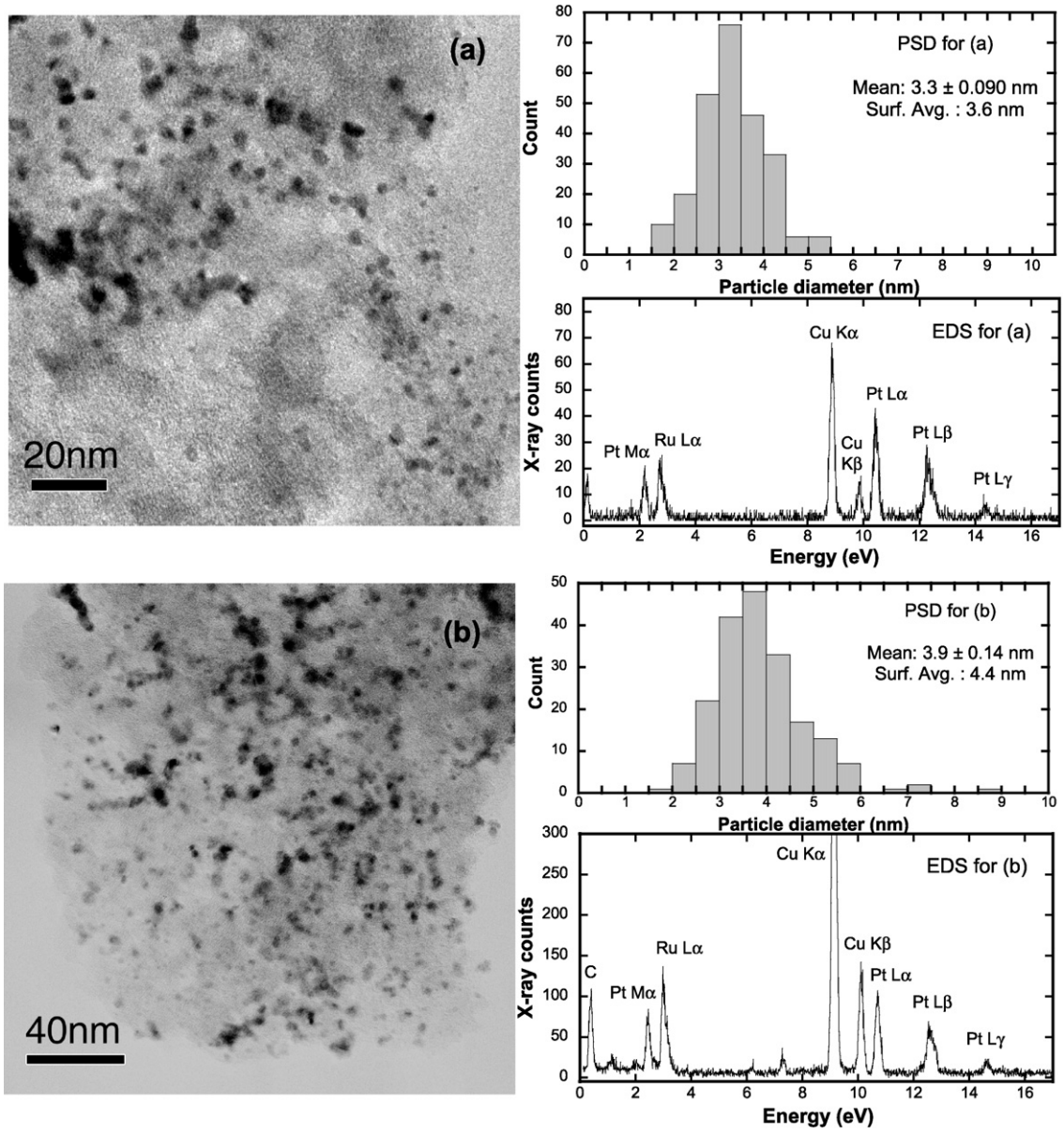

Fig. 1. TEM micrographs and corresponding PSDs and EDS spectra for PtRu/C (a) fresh and (b) recovered after use for glycerol hydrogenolysis in 0.8 M NaOH at 473 K and 40 bar H_2.

surface-averaged particle diameter from 2.8 to 4.6 nm as a result of aqueous-phase treatment.

The Fourier transforms presented in Figs. 4a and 4b illustrate the Pt and Ru interaction in the bimetallic sample after reduction in H_2 (g). The structure around Ru did not appear to be significantly altered from that of the Ru bulk reference (Fig. 4a). Because the Ru–Ru first-shell CN reported in Table 2 did not vary from Ru/C to PtRu/C, the Ru particles were not altered by the deposition of Pt; however, comparison of the Fourier transform of the PtRu/C sample with the Pt foil (Fig. 4b) revealed interaction of Pt with Ru. The Pt–Ru first-shell CN was 2.2 out of a total Pt first-shell CN of 7.8 (from Pt–Pt and Pt–Ru), indicating a substantial presence of Ru in the average first coordination sphere of Pt. It is interesting to note that the total first-shell Pt CN did not change significantly when the PtRu/C sample was treated under aqueous-phase conditions. A slight increase in the average particle size was observed by TEM of the fresh PtRu/C and of the catalyst recovered after use in the hydrogenolysis of glycerol in 0.8 M NaOH at 473 K and 40 bar H_2. Fig. 1b illustrates a broader PSD for PtRu/C recovered after catalysis, with the mean particle diameter increasing from 3.3 to 3.9 nm, and the surface-averaged particle diameter increasing from 3.6 to 4.4 nm after treatment in the aqueous phase. The TEM and EXAFS results both show that sintering of metal particles due to aqueous-phase processing was not as severe on the bimetallic PtRu/C sample as the monometallic Pt/C sample. Apparently, the Ru particles were able to stabilize the Pt against coalescence and sintering.

The Fourier transforms presented in Figs. 5a and 5b illustrate the extent of Au and Ru interaction for the AuRu/C bimetallic sample after reduction in H_2. Similar to the PtRu/C sample, the Ru particles maintained a structure corresponding to the

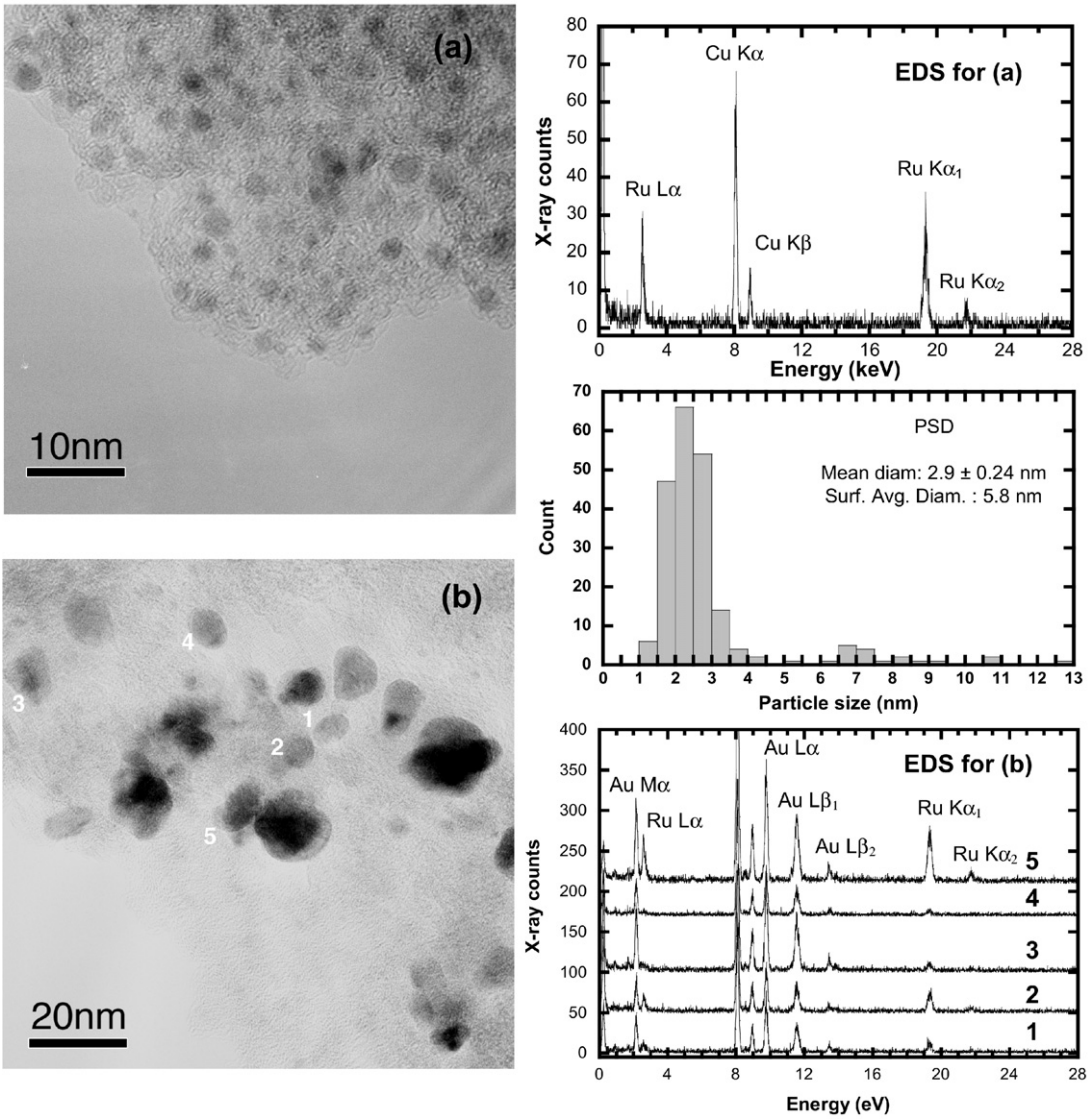

Fig. 2. TEM micrographs of AuRu/C with corresponding PSD and EDS spectra. (a) Particles in the range of 1.5–3 nm consist primarily of monometallic Ru; the EDS spectrum was taken from a ∼80 nm diameter circular area and is shown to the right of the micrograph. (b) Particles in the 5–10 nm range contain both Au and Ru; the EDS spectra of five individual particles are presented to the right of the micrograph.

Ru bulk reference (Fig. 5a). The Ru–Ru first-shell CN was 8.9 in comparison to the Ru–Au first-shell CN of 0.1, indicating very poor interaction of Au with Ru, on average. The Fourier transform of the Au EXAFS for the AuRu/C sample in Fig. 5b showed a slight modification of the Au structure on the bimetallic catalyst compared with Au foil. Fitting results for the catalyst resulted in a Au–Au first-shell CN of 6.9 and a Au–Ru first-shell CN of 1.0, indicating poor interaction of Au with Ru. Moreover, these EXAFS results are consistent with those from TEM and EDS showing that the sample contained bimetallic particles of Au and Ru in addition to monometallic particles of Ru and Au. Inspection of Fig. 5d and the structural parameters reported for the AuRu/C sample after treatment B in Table 2 showed further structural changes of the catalyst due to aqueous-phase processing.

A structure-sensitive probe reaction also can be used to ascertain whether or not the surface of our Ru catalyst has been modified by the addition of Pt or Au. The hydrogenolysis of ethane to methane is a well-known structure-sensitive reaction on Ru [15]. Fig. 6 summarizes the activity results of the various catalysts in the hydrogenolysis of ethane at 473 K. Equivalent masses of the Ru/C and the bimetallic PtRu/C and AuRu/C catalysts were used in these studies to maintain a constant Ru loading. In the studies of the monometallic Pt/C and the physical mixture of the Ru/C and Pt/C catalysts, the amount of Pt/C used was determined by matching the amount of surface Pt to that present in the bimetallic PtRu/C catalyst (assuming that all Pt was present on the surface). The amount of Au/C used in the studies of the monometallic Au/C catalyst and the physical mixture of Au/C and Ru/C was determined by matching the total metal loading of Au present in the AuRu/C catalyst. A turnover frequency (TOF) for ethane hydrogenolysis of 0.049 $\pm$ 0.0055 s^{-1} was obtained on Ru/C, which is comparable to a rate of ∼0.03 s^{-1} extrapolated from the work of Doi et al., who

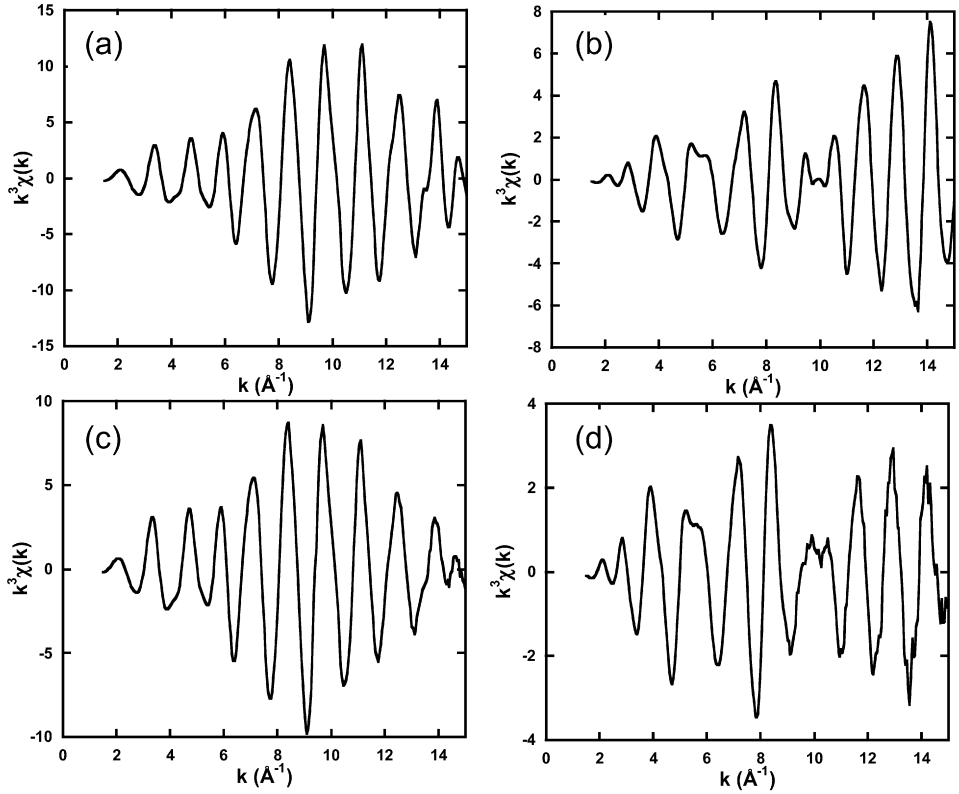

Fig. 3. Experimental χ data with k^3 weighting for sample PtRu/C; (a, c) Ru K-edge and (b, d) Pt L_{III}-edge. Treatments, (a, b) 1 atm H_2 at 298 K, following reduction at 473 K; (c, d) aqueous hydrogenolysis conditions, 0.4 M NaOH, 40 atm H_2, at 473 K.

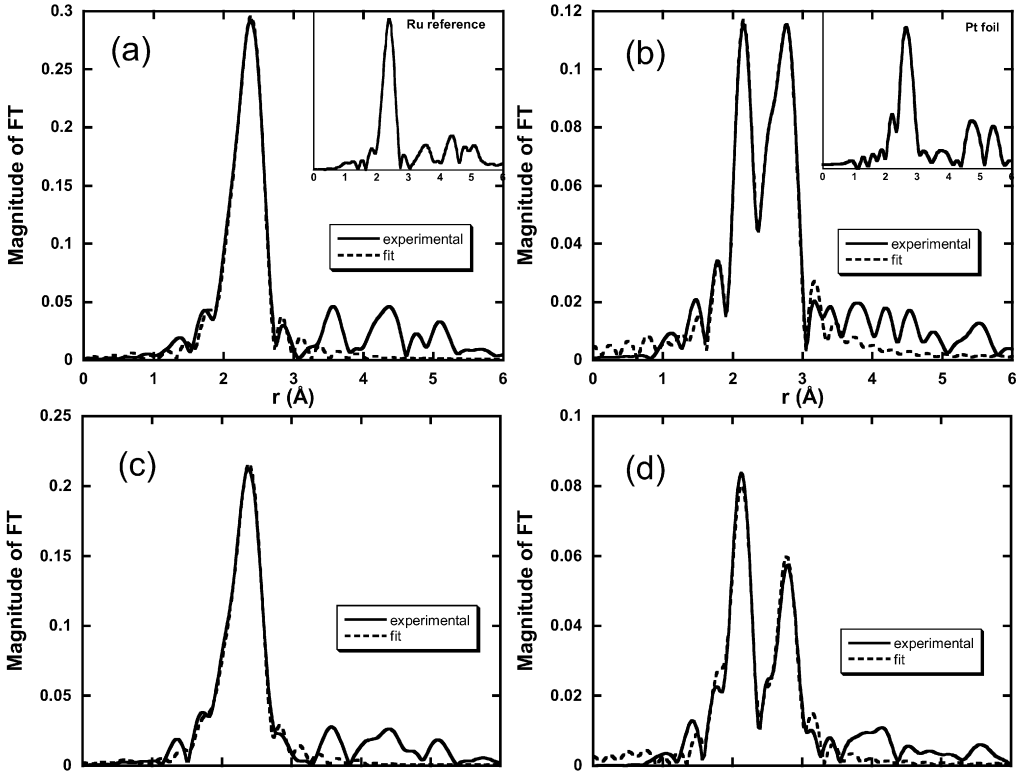

Fig. 4. Magnitude of the Fourier transformed k^3-weighted χ function (not corrected for phase shifts) with non-linear least squares fits for sample PtRu/C; (a, c) Ru K-edge (Ru–Ru and Ru–Pt shells) and (b, d) Pt L_{III}-edge (Pt–Pt and Pt–Ru shells). Treatments: (a, b) 1 atm H_2 at 298 K, following reduction at 473 K; (c, d) aqueous hydrogenolysis conditions, 0.4 M NaOH, 40 atm H_2, at 473 K.

Table 2
Structural parameters for monometallic and bimetallic catalysts derived from EXAFS

Catalyst	Treatment[a]	Absorber-scatterer	1st-shell CN	Interatomic distance (Å)	$\Delta\sigma^2$ (Å^2)	ΔE_0 (eV)
Ru/C	A	Ru–Ru	8.8	2.65	0.0079	1.9
Pt/C	A	Pt–Pt	8.6	2.74	0.0077	3.4
Pt/C	B	Pt–Pt	10.4	2.75	0.0082	4.4
PtRu/C	A	Ru–Ru	8.4	2.66	0.0066	3.7
		Ru–Pt	0.5	2.70	0.0037	3.7
		Pt–Ru	2.2	2.70	0.0037	4.3
		Pt–Pt	5.4	2.73	0.0060	4.3
PtRu/C	B	Ru–Ru	9.0	2.66	0.0084	2.6
		Ru–Pt	0.4	2.69	0.0044	2.6
		Pt–Ru	2.0	2.69	0.0044	3.1
		Pt–Pt	5.8	2.72	0.0090	3.1
AuRu/C	A	Ru–Ru	8.9	2.66	0.0068	3.2
		Ru–Au	0.1	2.72	0.013	3.2
		Au–Ru	1.0	2.72	0.013	−1.0
		Au–Au	6.9	2.84	0.0091	−1.0
AuRu/C	B	Ru–Ru	9.1	2.65	0.0077	2.0
		Ru–Au	0	–	–	–
		Au–Ru	0	–	–	–
		Au–Au	9.6	2.83	0.014	−2.4

[a] (A) 1 bar H_2 at 298 K, following reduction at 473 K; (B) aqueous-phase treatment: 0.4 M NaOH, 40 bar H_2, at 473 K.

studied the hydrogenolysis of ethane over a Ru/SiO_2 catalyst at comparable reaction conditions [40].

The activity of Pt/C could not be determined under our hydrogenolysis conditions, presumably because of the low loading of Pt in the system. Under similar reaction conditions, a Pt/SiO_2 catalyst was found to be approximately three orders of magnitude less active than Ru/SiO_2 for ethane hydrogenolysis [40,41]. Therefore, given the low loadings of Pt/C, any conversion of ethane to methane likely fell below the detection limits of our system.

A physical mixture of the monometallic Ru/C and Pt/C catalysts exhibited a TOF similar to the Ru/C, however, the TOF of the physical mixture was based solely on the Ru contribution, because Pt was effectively inactive for ethane hydrogenolysis. Therefore, in studies involving a physical mixture of the catalysts, the TOF was determined by the rate of methane formation per surface Ru atom as determined by H_2 chemisorption. Interestingly, the PtRu/C catalyst gave a TOF of $0.039 \pm 0.0047\ s^{-1}$, which was not significantly lower than the value for the Ru/C catalyst or the physical mixture of the two monometallic catalysts. Because the TEM and EDS analyses detected bimetallic Pt–Ru particles, and EXAFS indicated an interaction between the Ru and Pt, we expected the Pt to substantially depress the activity of the PtRu/C catalyst. One possible explanation for the observed activity of the PtRu/C catalyst is that the Pt and Ru were acting cooperatively. It has been suggested that in bimetallic systems, each metal can separately activate a different reactant, and, thereafter, surface diffusion allows for migration and reaction of the activated species to form the product [42]. Ethane hydrogenolysis on the monometallic catalysts revealed that Ru is much more efficient than Pt for C–C cleavage; however, the H_2 chemisorption indicated that both metals had equivalent capacity for dissociative adsorption of H_2. It is possible that for the PtRu bimetallic system, C–C cleavage of ethane occurred on Ru, whereas H_2 adsorption occurred on Pt adjacent to Ru.

In agreement with previous studies [22], we found that the Au/C catalyst was inactive for ethane hydrogenolysis. A physical mixture of the Ru/C and Au/C yielded a TOF comparable to that of the Ru/C monometallic catalyst, again where the TOF of the mixture was based solely on the Ru contribution, due to the inactivity of Au. However, the bimetallic AuRu/C displayed a TOF of $0.011 \pm 0.0020\ s^{-1}$, indicating a more than fourfold decrease in activity compared with the Ru/C catalyst. These activity results corroborated those from H_2 chemisorption, TEM, and EXAFS, all of which demonstrated that Au modified the surface of Ru.

We then evaluated the activity of the bimetallic PtRu/C and AuRu/C catalysts in the aqueous-phase hydrogenolysis of glycerol both under neutral conditions and in the presence of base. The results of these studies are summarized in Table 3. The overall turnover frequency ($TOF_{overall}$) is reported as the rate of glycerol converted at approximately 20% conversion per surface metal atom as determined by H_2 chemisorption. For runs involving a physical mixture of the monometallic catalysts, the total number of surface metal atoms was determined from the individual contributions of Ru/C and Pt/C to the mixture. The carbon balance is given as the percentage of carbon accounted for in the system (both liquid and gas phases) at the end of 5 h. The amount of missing carbon in the system can be explained by a loss of gas-phase products during sampling of the reaction mixture. Because the reactor system was not equipped to separate and analyze the gas and liquid phase products simultaneously, a small amount of gas-phase products inevitably was lost during liquid sampling. Thus, larger errors in the material balance would be expected for runs with larger gas-phase product inventories. The product selectivities of the reactions are summarized in Table 4. The selectivities are reported at approximately 20% conversion of glycerol and after the reaction

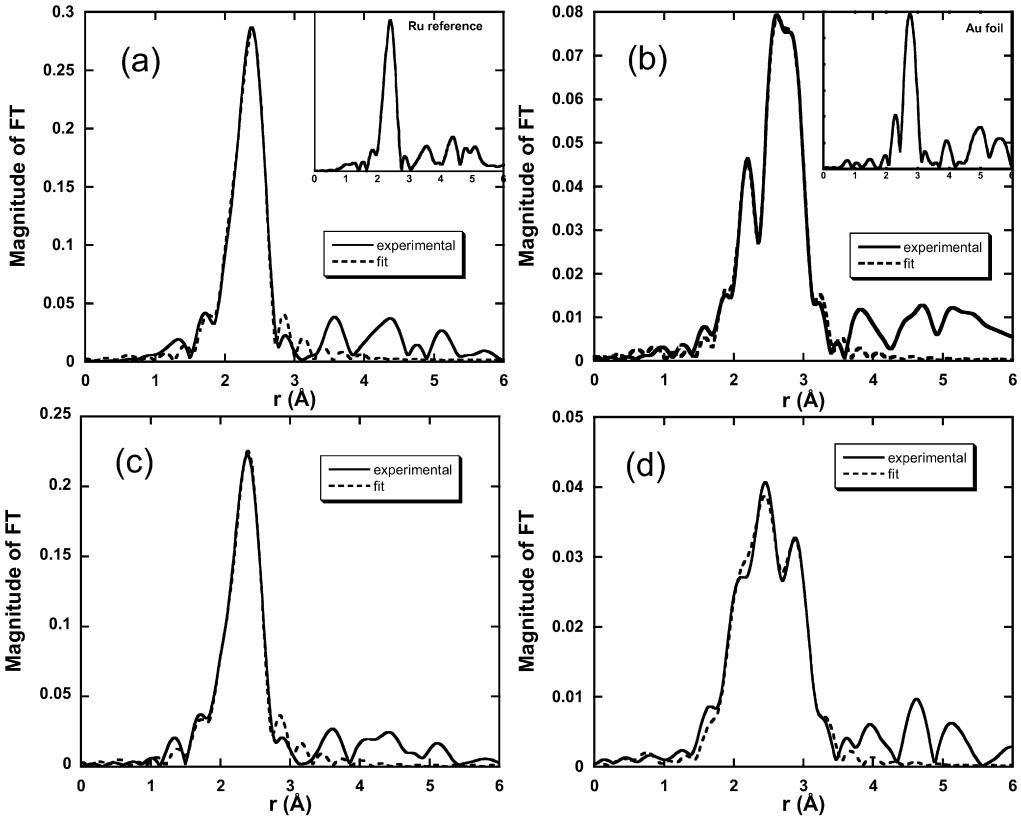

Fig. 5. Magnitude of the Fourier transformed k^3-weighted χ function (not corrected for phase shifts) with non-linear least squares fits for sample AuRu/C; (a, c) Ru K-edge and (b, d) Au L_{III}-edge. Treatments: (a, b) 1 bar H_2 at 298 K, following reduction at 473 K; (c, d) aqueous hydrogenolysis conditions, 0.4 M NaOH, 40 bar H_2, at 473 K.

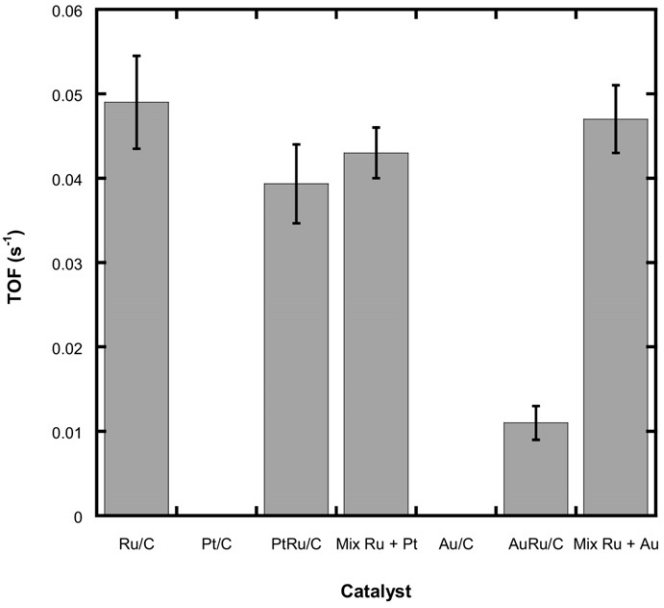

Fig. 6. Turnover frequencies for the hydrogenolysis of ethane at 473 K over monometallic, bimetallic, and physical mixtures of the catalysts. Error bars represent 95% confidence limits.

was stopped at 5 h. The selectivity of each product was based on the carbon selectivity, where

$$\text{selectivity} = \frac{\text{moles of carbon in specific product}}{\text{moles of carbon in all observed products}}.$$

The conversion of glycerol under neutral conditions on the Ru-, Pt-, and Au-containing catalysts is shown in Fig. 7. Comparison of the TOFs reported in runs 1, 2, and 3 of Table 3 together with the conversion profiles shown in Fig. 7, demonstrate that under neutral conditions, Ru/C is more active than Pt/C and Au/C is completely inactive for the hydrogenolysis of glycerol. Because TEM and EXAFS analyses confirmed that aqueous-phase processing caused sintering of the Pt particles, the TOF based on surface Pt determined by H_2 chemisorption on a fresh catalyst may be underestimated. For this reason, the reaction rates normalized per total metal atoms are also reported in Table 3.

On a total metal basis, Ru/C was still superior to Pt/C and Au/C in glycerol hydrogenolysis under neutral conditions. This activity trend is the same as that for ethane hydrogenolysis. From the product selectivities reported in Table 4, Ru apparently favored the production of ethylene glycol, whereas Pt favored the production of propylene glycol under neutral conditions. This can be explained by the mechanism of glycerol hydrogenolysis presented in Scheme 1 [12]. In this mechanism, both metals catalyze the initial dehydrogenation of glycerol to glyceraldehyde; however, a metal-catalyzed C–C cleavage pathway leading to ethylene glycol formation is available on Ru that does not occur significantly on Pt, and thus, a base-catalyzed retro-aldol reaction accounts for C–C cleavage products in the presence of Pt. Over both metals, the scission of

Table 3
Rates of glycerol hydrogenolysis over monometallic and bimetallic catalysts[a]

Run #	Catalyst	Base	Conversion (%)[b]	Carbon balance[c]	$TOF_{overall.}$ (s^{-1})[d]	Rate × 10^3 (mol s^{-1} mol metal^{-1})[e]
1	Ru/C	None	40	84	0.02 ± 0.003	9.9
2	Pt/C	None	13	97	0.006 ± 0.002	2.5
3	Au/C	None	0	100	–	–
4	Ru/C + Pt/C[f]	None	44	81	0.02 ± 0.004[g]	7.8
5	Ru/C + Au/C[h]	None	25	95	0.01 ± 0.003	4.6
6	PtRu/C	None	42	78	0.05 ± 0.02	12
7	AuRu/C	None	25	92	0.03 ± 0.009	5.1
8	Ru/C	NaOH	100	85	0.2 ± 0.03	77
9	Pt/C	NaOH	92	83	0.3 ± 0.05	141
10	Ru/C + Pt/C[f]	NaOH	100	90	0.2 ± 0.04	102
11	PtRu/C	NaOH	100	91	0.3 ± 0.04	69
12	Ru/C + Au/C[h]	NaOH	100	88	0.2 ± 0.07	74
13	AuRu/C	NaOH	100	90	0.5 ± 0.05	80

[a] Reaction conditions: 1 wt% glycerol solution, 0.8 M NaOH (when used), $T = 473$ K, $P_{H_2} = 40$ bar.
[b] Conversion determined after 5 h.
[c] Percentage of carbon accounted for after 5 h of reaction.
[d] Overall rate determined at ∼20% conversion of glycerol. Error represents 95% confidence limits.
[e] Rate normalized by the total moles of metal in the catalyst.
[f] Physical mixture of the monometallic Ru/C and Pt/C, where the number of surface Pt atoms equals those present in the bimetallic PtRu/C (assuming all Pt was deposited on the surface of the PtRu/C catalyst).
[g] Rates were normalized by the appropriate contribution from Ru/C and Pt/C in the mixture.
[h] Physical mixture of the monometallic Ru/C and Au/C, where the total Au loading equals that present in the bimetallic AuRu/C.

Table 4
Product selectivities during glycerol hydrogenolysis[a]

Run #[b]	Catalyst	Base	Conversion (%)[c]	Carbon selectivity					
				EG	PG	LA	FA	CH_4[d]	CO_2[d]
1	Ru/C	None	17	0.68	0.32	0	0	–	–
			40	0.47	0.26	0	0	0.26	0.01
2	Pt/C	None	–	–	–	–	0	–	–
			13	0.17	0.79	0	0	0	0
4	Ru/C + Pt/C[e]	None	19	0.59	0.39	0	0	–	–
			44	0.41	0.39	0	0	0.18	0.01
5	Ru/C + Au/C[f]	None	19	0.50	0.50	0	0	–	–
			25	0.44	0.46	0	0	0.09	0.01
6	PtRu/C	None	23	0.70	0.30	0	0	–	–
			42	0.49	0.24	0	0	0.27	Trace
7	AuRu/C	None	18	0.65	0.35	0	0	–	–
			25	0.49	0.30	0	0	0.21	0
8	Ru/C	NaOH	25	0.13	0.36	0.47	0	–	–
			100	0.01	0.19	0.34	0.43	0.02	0.01[g]
9	Pt/C	NaOH	25	0.02	0.30	0.62	0	–	–
			92	0.02	0.47	0.49	0	0	0
10	Ru/C + Pt/C[e]	NaOH	23	0.11	0.49	0.37	0	–	–
			100	0.002	0.18	0.37	0.36	0.02	0.05[g]
11	PtRu/C	NaOH	22	0.15	0.37	0.41	0	–	–
			100	0.02	0.18	0.37	0.37	0.01	0.02[g]
12	Ru/C + Au/C[f]	NaOH	24	0.14	0.41	0.41	0	–	–
			100	0.01	0.20	0.35	0.39	0.02	0.02[g]
13	AuRu/C	NaOH	21	0.10	0.25	0.60	0	–	–
			100	0.001	0.12	0.38	0.44	0.01	0.03[g]

[a] Reaction conditions: 1 wt% glycerol solution, 0.8 M NaOH (when used), $T = 473$ K, $P_{H_2} = 40$ bar. EG: ethylene glycol; PG: propylene glycol; LA: lactate; FA: formate.
[b] Run numbers are the same as those listed in Table 3.
[c] Carbon selectivities were determined both at ∼20% conversion of glycerol and at the final conversion attained after 5 h of reaction.
[d] The gas phase was only sampled after the completion of the reaction. Therefore gas phase compositions at 20% conversion of glycerol are not available.
[e] Physical mixture of the monometallic Ru/C and Pt/C, where the number of surface Pt atoms equals those present in the bimetallic PtRu/C (assuming all Pt was deposited on the surface of the PtRu/C catalyst).
[f] Physical mixture of the monometallic Ru/C and Au/C, where the total Au loading equals that present in the bimetallic AuRu/C.
[g] In the form of carbonate.

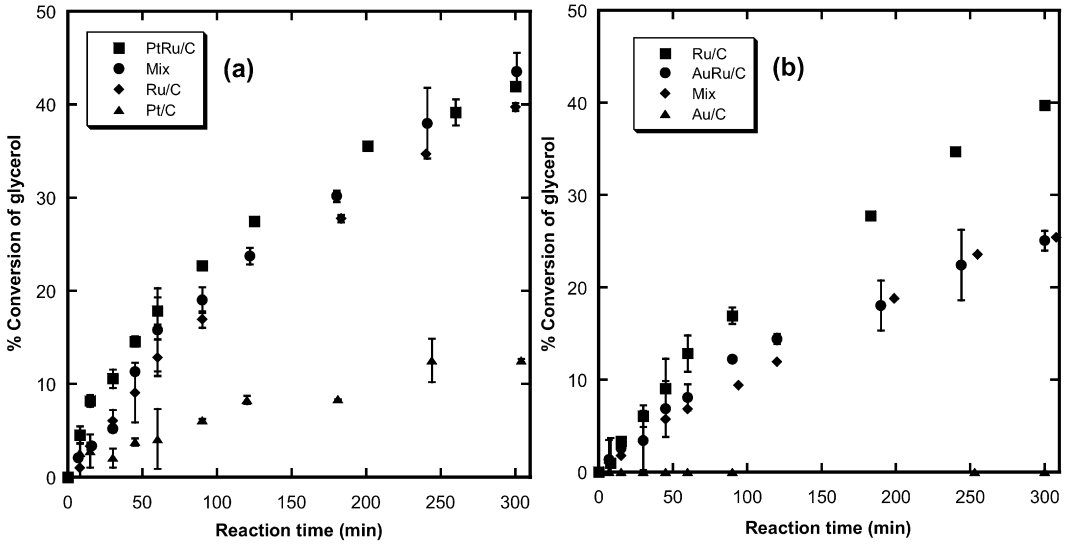

Fig. 7. Conversion of glycerol under neutral conditions at 473 K and 40 bar H_2 on (a) Ru- and Pt-containing catalysts and (b) Ru- and Au-containing catalysts. Error bars represent 95% confidence limits.

C–O bonds leading to propylene glycol formation is attributed to a base-catalyzed dehydration reaction.

The physical mixture of Ru/C and Pt/C (run 4 in Tables 3 and 4) had initial activity and selectivity comparable to that of the Ru/C monometallic catalyst, which is expected because Pt/C was significantly less active than Ru/C under neutral conditions. Interestingly, the bimetallic PtRu/C catalyst also exhibited activity and selectivity similar to that of the monometallic Ru/C catalyst. Again, these results are similar to those of our earlier ethane hydrogenolysis study, in which we found that although Pt/C was relatively inactive for hydrogenolysis, PtRu/C and Ru/C displayed similar activity. As in the case of ethane hydrogenolysis, we propose that Pt and Ru catalyze separate steps of the reaction. In a study of the liquid-phase hydrogenation of 2-butanone on carbon-supported Pt–Ru bimetallic catalysts, Breen et al. observed that the bimetallic catalysts were more than twice as active as the sum of the activities of the monometallic catalysts [18]. They suggested that the presence of Pt clusters on the Ru surface could enhance the dissociative adsorption of H_2, which, if competitive adsorption between H_2 and 2-butanone were a rate-determining process, could enhance the overall kinetics of the reaction. Applying similar reasoning to our system, it is possible that the presence of Pt provided sites for dissociative adsorption of H_2, whereas Ru provided sites for glycerol adsorption and C–C cleavage. Although Pt/C itself was less active for glycerol hydrogenolysis, Pt-modified Ru could be as active as a monometallic Ru/C catalyst.

Inspection of Fig. 7b and runs 5 and 7 in Table 3 reveals that the addition of Au decreased the hydrogenolysis activity of Ru/C. However, modifying the Ru surface with Au was almost the same as a physical mixture of the two monometallic catalysts. Note that the TOF reported for run 7 in Table 3 was determined using the metal dispersion obtained from H_2 chemisorption. Nonetheless, TEM of the AuRu/C recovered after use in this reaction showed a change in the particle morphology as a result of aqueous-phase processing. After reaction, there was a bimodal PSD of the AuRu/C catalyst. The as-prepared catalyst had ∼82% of the particles in the 1.5–3 nm range; in contrast, the AuRu/C recovered after use in the hydrogenolysis of glycerol under neutral conditions had only 48% of the particles in that size range. Similarly, the as-prepared AuRu/C catalyst contained only ∼8% of 6–10 nm particles, compared with 42% in the AuRu/C catalyst recovered after reaction. Furthermore, the density of >10-nm particles also increased after reaction, with these particles containing primarily Au. Apparently, the aqueous-phase reaction conditions promoted sintering of the Au particles. The TOF for run 7 based on characterization of a fresh catalyst is perhaps an overestimation; the Au initially present on Ru apparently moved off the surface and aggregated, thus exposing additional Ru to the reaction medium. Normalizing the rate per total metal loading in the catalyst reveals a closer agreement between the rate of hydrogenolysis on the physical mixture of Ru/C and Au/C (run 5) and the bimetallic AuRu/C catalyst (run 7). The product selectivities reported in Table 4 for AuRu/C and Ru/C were also quite similar; both favored ethylene glycol production over propylene glycol production, with significant production of methane. Interestingly, the physical mixture of Ru/C and Au/C, although less active than Ru/C alone, had a slightly greater selectivity to propylene glycol with decreased formation of methane.

Fig. 8 presents the glycerol reaction profile over the various catalysts in 0.8 M NaOH. The presence of base is known to significantly enhance the rate of glycerol hydrogenolysis [43–45]. We previously reported that the extent of enhancement is greater for Pt/C than Ru/C [12], as shown in runs 1, 2, 8, and 9 in Table 3. Whereas direct comparison of the TOFs for these reactions is somewhat misleading due to the sintering of Pt particles on the carbon support, the normalized rates still show that the initial activity of Pt was enhanced by base to a greater extent than Ru. Inspection of the product selectivities for Ru/C and Pt/C reported in Table 4 shows that in the presence of base (entries 8 and 9), lactate was the major product formed during

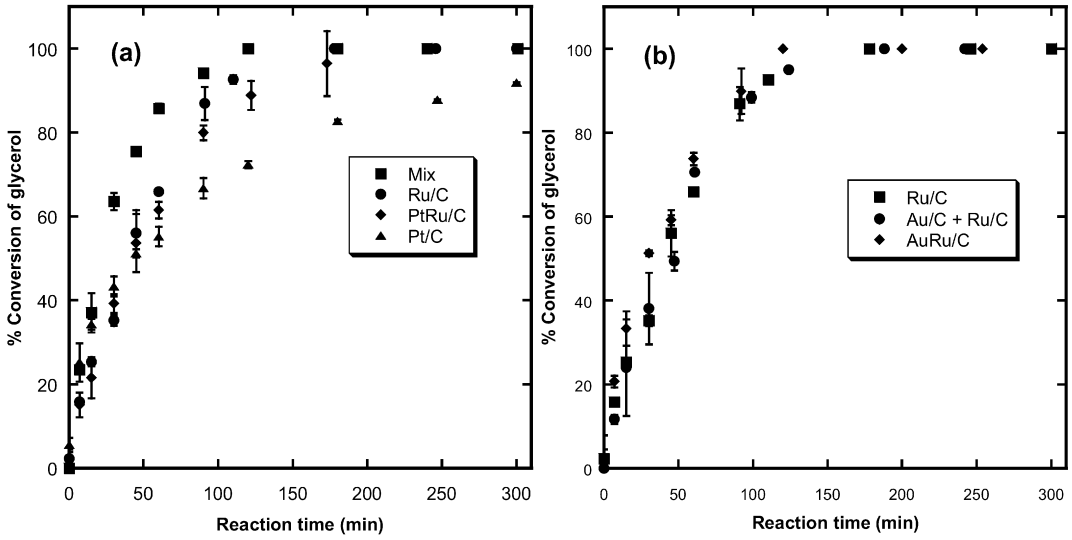

Fig. 8. Conversion of glycerol in the presence of 0.8 M NaOH at 473 K and 40 bar H_2 over (a) Ru-, Pt-containing catalysts and (b) Ru- and Au-containing catalysts. Error bars represent 95% confidence limits.

glycerol hydrogenolysis. Propylene glycol was the next most abundant product formed on both catalysts at low conversions (25%). Although ethylene glycol was no longer a major product formed on Ru/C, its selectivity at high pH was still higher than that on Pt/C (runs 8 and 9 in Table 4). Furthermore, the products formate, methane, and carbonate were produced over Ru/C at high glycerol conversion but were not formed over Pt/C.

The initial activity of PtRu/C (run 11 of Table 3) for glycerol hydrogenolysis was similar to that of the Ru/C in the presence of base, as depicted in Fig. 8a. Inspection of runs 10 and 11 of Table 4 also shows that both the physical mixture of Ru/C and Pt/C and the bimetallic PtRu/C exhibited similar product selectivities to the monometallic Ru/C (run 8) in the presence of base. One possible explanation for these similar product selectivities is that the Pt and Ru particles segregated under the aqueous-phase processing conditions. To evaluate this hypothesis, TEM was performed on the PtRu/C catalyst recovered after use in the hydrogenolysis of glycerol in the presence of 0.8 M NaOH, as shown in Fig. 1b. Because EDS analysis of more than 10 individual particles confirmed the presence of both Ru and Pt, the 2 metals apparently did not separate on the carbon support during aqueous-phase processing. In situ EXAFS of the PtRu/C sample provided further evidence that the Pt and Ru particles remained intact as bimetallic clusters during aqueous-phase processing. Inspection of the Fourier transforms at the Pt L_{III}-edge shown in Fig. 4d indicates that even in the aqueous phase, under basic conditions, there was still significant interaction of Pt with Ru. Furthermore, the first-shell CNs for Ru–Pt and Pt–Ru reported in Table 2 remained relatively unchanged as a function of pretreatment. These results, which agree with those from TEM, confirm that Pt and Ru particles did not migrate substantially during glycerol hydrogenolysis. Evidently, modification of the Ru surface with Pt did not alter the activity or selectivity for glycerol hydrogenolysis, a conclusion similar to that derived from ethane hydrogenolysis.

Comparing the activity results for Ru and Au catalysts (runs 8, 12, and 13 of Table 3 and inspection of Fig. 8b) used for glycerol hydrogenolysis in the presence of 0.8 M NaOH, the AuRu/C bimetallic catalyst as well as a physical mixture of the monometallic Ru/C and Au/C catalysts exhibited comparable rates. In addition, the product selectivities also were similar, as reported in Table 4. Because the modification of Ru with Au resulted in decreased activity for ethane hydrogenolysis, we anticipated a corresponding decrease in rate for glycerol hydrogenolysis. However, the glycerol hydrogenolysis rate was not decreased by Au, suggesting that the Au may have migrated off the Ru surface during reaction in the aqueous phase. Indeed, TEM and EDS of the AuRu/C catalyst recovered after use in the hydrogenolysis of glycerol in 0.8 M NaOH revealed segregated regions of monometallic Ru and Au. The small particles observed by TEM were composed of Ru, and the larger particles were exclusively Au. The change in first-shell CNs reported in Table 2 also supports this hypothesis. Whereas treatment of the sample in H_2 (g) resulted in a Ru–Au first-shell CN of 0.1 and an Au–Ru first-shell CN of 1.0, exposure of the sample to a H_2-saturated basic solution resulted in complete loss of the Ru–Au interaction detected by EXAFS. Therefore, during glycerol hydrogenolysis, Au appeared to move from the Ru surface to the carbon support. Because the remaining Ru particles were still highly dispersed, the activity and selectivity of AuRu/C were similar to those of the parent monometallic Ru/C.

4. Conclusion

Activated carbon-supported bimetallic PtRu and AuRu catalysts were prepared by surface redox reactions for use in the aqueous-phase hydrogenolysis of glycerol. Results from characterization by H_2 chemisorption, analytical electron microscopy, and X-ray absorption spectroscopy confirmed that Pt or Au was successfully deposited on supported Ru particles. In the case of PtRu/C, TEM and EDS showed the presence of relatively small bimetallic Pt–Ru particles with a narrow PSD (mean diameter ∼3.3 nm). Both TEM of the PtRu/C catalyst recovered after use in the hydrogenolysis of glycerol in the pres-

ence of 0.8 M NaOH and in situ XAS of PtRu/C under an H_2-saturated basic solution revealed that the Pt and Ru remained in close contact, indicating that segregation of the metals did not occur during reaction. Modification of the Ru surface with Pt did not alter the catalytic activity of PtRu/C for ethane or glycerol hydrogenolysis compared with the monometallic Ru/C.

TEM and EDS showed that the as-prepared AuRu/C catalyst had a broader PSD than the PtRu/C; however, individual particles containing both Ru and Au were observed. These results were corroborated by X-ray absorption spectroscopy. The hydrogenolysis of ethane, a structure-sensitive probe reaction, confirmed that Au modified a fraction of the Ru surface atoms; however, the activity and selectivity of AuRu/C in the hydrogenolysis of glycerol was similar to the monometallic Ru/C. The activity results, coupled with postreaction characterization, strongly suggest that Au migrates off of Ru during glycerol hydrogenolysis and agglomerates on the support.

Both bimetallic catalysts, PtRu/C and AuRu/C, favored the formation of ethylene glycol over propylene glycol during glycerol hydrogenolysis in neutral pH conditions. In the presence of base, the bimetallic catalysts favored the production of lactate and propylene glycol over ethylene glycol. The product selectivities over the bimetallic catalysts at both high pH and neutral conditions were quantitatively similar to those observed over the monometallic Ru catalyst.

Acknowledgments

This work was supported by the National Science Foundation (Grants CTS-0313484 and CTS-0624608). Research was carried out on beamline X-18B (operated by the Synchrotron Catalysis Consortium, funded by US Department of Energy [DOE] Grant DE-FG02-05ER15688) at the National Synchrotron Light Source, Brookhaven National Laboratory, which is supported by the US DOE, Division of Materials Sciences and Division of Chemical Sciences, under Contract DE-AC02-98CH10886. Partial support also was provided by US DOE, Office of Basic Energy Sciences Grant DE-FG02-95ER14549.

References

[1] L.R. Lynd, C.E. Wyman, T.U. Gerngross, Biotechnol. Progr. 15 (1999) 777.
[2] B.E. Dale, J. Chem. Technol. Biotechnol. 78 (2003) 1093.
[3] B. Kamm, M. Kamm, Appl. Microbiol. Biotechnol. 64 (2004) 137.
[4] A.J. Ragauskas, C.K. Williams, B.H. Davison, G. Britovsek, J. Cairney, C.A. Eckert, W.J. Frederick, J.P. Hallett, D.J. Leak, C.L. Liotta, J.R. Mielenz, R. Murphy, R. Templer, T. Tschaplinski, Science 311 (2006) 484.
[5] T. Werpy, G. Petersen, US DOE Report: Top Value Added Chemicals from Biomass, Vol. 1: Results of Screening for Potential Candidates from Sugars and Synthesis Gas, 2004.
[6] C. Chiu, Ind. Eng. Chem. Res. 45 (2006) 791.
[7] ADM plans polyols unit using renewable feedstock (Archer Daniels Midland Co. to build renewable plant) (Brief article), Chem. Week 167 (1) (2005) 23.
[8] E. Chynoweth, ICIS Chem. Bus. (Weekly) 1 (1) (2006) 39.
[9] I.T. Clark, Ind. Eng. Chem. 50 (1958) 1125.
[10] C. Montassier, D. Giraud, J. Barbier, Polyol Conversion by Liquid Phase Heterogeneous Catalysis over Metals, Elsevier, Amsterdam, 1988, p. 165.
[11] D.K. Sohounloue, C. Montassier, J. Barbier, React. Kinet. Catal. Lett. 22 (1983) 391.
[12] E.P. Maris, R.J. Davis, J. Catal. 249 (2007) 328.
[13] C. Montassier, J.C. Menezo, L.C. Hoang, C. Renaud, J. Barbier, J. Mol. Catal. 70 (1991) 99.
[14] D.G. Lahr, B.H. Shanks, J. Catal. 232 (2005) 386.
[15] J.H. Sinfelt, Bimetallic Catalysts: Discoveries, Concepts, and Applications, Wiley, New York, 1983.
[16] C. Montassier, J.C. Menezo, J. Moukolo, J. Naja, L.C. Hoang, J. Barbier, J.P. Boitiaux, J. Mol. Catal. 70 (1991) 65.
[17] C. Montassier, J.C. Menezo, J. Naja, P. Granger, J. Barbier, P. Sarrazin, B. Didillon, J. Mol. Catal. 91 (1994) 119.
[18] J.P. Breen, R. Burch, K. Griffin, C. Hardacre, M. Hayes, X. Huang, S.D. O'Brien, J. Catal. 236 (2005) 270.
[19] Y.J. Zhang, A. Maroto-Valiente, I. Rodriguez-Ramos, Q. Xin, A. Guerrero-Ruiz, Catal. Today 93–95 (2004) 619.
[20] E. Antolini, L. Giorgi, F. Cardellini, E. Passalacqua, J. Solid State Electrochem. 5 (2001) 131.
[21] H. Okamoto, P.R. Subramanian, L. Kacprzak, Binary Alloy Phase Diagrams, in: T.B. Massalaski (Ed.), ASM International, USA, 1990.
[22] S. Galvagno, J. Schwank, G. Parravano, F. Garbassi, A. Marzi, G.R. Tauszik, J. Catal. 69 (1981) 283.
[23] A.G. Shastri, J. Schwank, J. Catal. 95 (1985) 271.
[24] A.G. Shastri, J. Schwank, J. Catal. 95 (1985) 284.
[25] P. Gallezot, N. Nicolaus, G. Fleche, P. Fuertes, A. Perrard, J. Catal. 180 (1998) 51.
[26] B.P. Block, J.C. Bailar, J. Am. Chem. Soc. 73 (1951) 4722.
[27] J. Barbier, P. Marecot, G. Delangel, P. Bosch, J.P. Boitiaux, B. Didillon, J.M. Dominguez, I. Schifter, G. Espinosa, Appl. Catal. A 116 (1994) 179.
[28] C.L. Pieck, P. Marecot, J. Barbier, Appl. Catal. A 143 (1996) 283.
[29] C.L. Pieck, P. Marecot, J. Barbier, Appl. Catal. A 134 (1996) 319.
[30] C.E. Fiori, C.R. Swyt, R.L. Myklebust, Desktop Spectrum Analyzer (Program), National Institute of Standards and Technology, Gaithersburg, MD, 1992.
[31] W. Rasband, ImageJ Software v. 1.37 (program), National Institute of Health, http://rsb.info.nih.gov/ij/.
[32] E.P. Maris, W.C. Ketchie, V. Oleshko, R.J. Davis, J. Phys. Chem. B 110 (2006) 7869.
[33] T. Ressler, WinXAS v. 2.33 (program), Berlin, 2001.
[34] A.L. Aunkudinov, C. Bouldin, J.J. Rehr, J. Sims, H. Hung, Phys. Rev. B 65 (2002) 104107.
[35] D.C. Koningsberger, B.L. Mojet, G.E. van Dorssen, D.E. Ramaker, Top. Catal. 10 (2000) 143.
[36] G.H. Via, K.F. Drake, G. Meitzner, F.W. Lytle, J.H. Sinfelt, Catal. Lett. 5 (1990) 25.
[37] X. Wu, B.C. Gerstein, T.S. King, J. Catal. 123 (1990) 43.
[38] A. Jentys, Phys. Chem. Chem. Phys. 1 (1999) 4059.
[39] W.C. Ketchie, E.P. Maris, R.J. Davis, Chem. Mater. 19 (2007) 3406.
[40] Y. Doi, H. Miyake, K. Soga, J. Mol. Catal. 48 (1988) 123.
[41] R.D. Cortright, R.M. Watwe, J.A. Dumesic, J. Mol. Catal. A 163 (2000) 91.
[42] R.D. Adams, J. Organomet. Chem. 600 (2000) 1.
[43] B. Casale, A.M. Gomez, US Patent 5 276 181 (1994).
[44] L. Schuster, M. Eggersdorfer, US Patent 5 616 817 (1997).
[45] D.G. Lahr, B.H. Shanks, Ind. Eng. Chem. Res. 42 (2003) 5467.